HiSST: International Conference on
High-Speed Vehicle Science Technology
26–29 November 2018, Moscow, Russia

Study on ramjet mode of variable geometry RBCC at low Mach number via full flow path simulations

Hongliang Pan[1], *Jinying Ye*[2], *Fei Qin*[3], *Yajun Wang*[4]

Abstract

The use of a structurally variable combustor is one of the most effective methods to improve the performance of a rocket-based combined-cycle (RBCC) engine over a wide operating range. This paper aims to study the matching between the combustor and the inlet/exhaust of a variable geometry RBCC engine at low inflow Mach numbers, furthermore the paper focus on the feasibility of using a variable geometry combustor to carry out a steady secondary fuel combustion in a pure ramjet mode instead of in a rocket aided ramjet mode in order to improve the engine performance at low inflow Mach number stage. Under the inflow conditions of Ma 2 and Ma 3, the matching operating conditions between the combustor and the inlet/exhaust are studied in detail based on the rocket-ramjet combustion mode. Different combustion organization methods show that the performance of the engine can be optimized by the fuel pylons concentrated injection under the Ma 3 inflow condition. By injecting secondary fuel in the isolator section, the transition of the engine from the rocket-ramjet mode to the pure ramjet mode is obtained in the variable geometry ram combustor. In the pure ramjet mode, the specific impulse of the engine is increased by 14.5% compared with in the rocket-ramjet mode, despite the ram specific impulse decreased by 10.2% due to a worsen combustion efficiency without rocket jet.

Keywords: *Variable geometry, RBCC, ramjet mode, numerical simulation*

Nomenclature

Latin

A – Pre-exponential factor, $(kmol/m^3)^{1-\eta F-\eta O}/s$
b – Temperature exponent, Dimensionless
E – Activation energy, J/kmol
ER – Fuel equivalent ratio, Dimensionless
F – Thrust of the engine, N
F_{ram} –Thrust of the ramjet, N
F_{rocket} –Thrust of the primary rocket, N
g_o – Gravitational acceleration, m/s^2
I_{sp} – Engine specific impulse, s
$I_{sp\text{-}ram}$ – Ram specific impulse, s
Ma – Mach number, Dimensionless
Ma_0 – Flight Mach number, Dimensionless
$\dot{m}_{fuel}$ –Mass flow rate of the secondary fuel, kg/s
$\dot{m}_{rocket}$ –Mass flow rate of the primary rocket, kg/s
p – Static pressure, Pa
p_0 – Total pressure at the isolator inlet, Pa
p_{in} – Static pressure at the isolator inlet, Pa
T_{AFT} – Adiabatic flame temperature, K
T_t – Total temperature, K
T_{ti} – Total temperature at isolator inlet, K

Greek

η_b – Combustion efficiency, Dimensionless
η_F – Exponent of the fuel mole fraction, Dimensionless
η_O – Exponent of the oxidizer mole fraction, Dimensionless

[1] *Science and Technology on Combustion, Internal Flow and Thermo-structure Laboratory, Northwestern Polytechnical University, Xi'an, China, 710072, panhl@nwpu.edu.cn*
[2] *Science and Technology on Combustion, Internal Flow and Thermo-structure Laboratory, Northwestern Polytechnical University, Xi'an, China, 710072, yejy060620@mail.nwpu.edu.cn*
[3] *Science and Technology on Combustion, Internal Flow and Thermo-structure Laboratory, Northwestern Polytechnical University, Xi'an, China, 710072, qinfei@nwpu.edu.cn*
[4] *Science and Technology on Combustion, Internal Flow and Thermo-structure Laboratory, Northwestern Polytechnical University, Xi'an, China, 710072, wangyajun@nwpu.edu.cn*

1. Introduction

Rocket-based combined-cycle (RBCC) engine is a combined propulsion system that operates in a wide flight envelop with multi-missions. It integrates a high thrust-to-weight ratio, low specific impulse rocket engine with a low thrust-to-weight ratio, high specific impulse dual-mode ramjet engine into a same flow path. It enables flight vehicles to take-off from zero speed to hypersonic flight, and is one of the major propulsion solutions for space transportation and hypersonic flight vehicle in near space [1-4]. Basically, the combustor configuration needs to be divergent in order to achieve a supersonic combustion between the incoming air and the secondary fuel injected into ram combustor in the scramjet mode, while to be convergent-divergent in order to conduct an efficient subsonic combustion of the secondary fuel in the ejector and ramjet modes[2]. Also the expansion ratio of the combustor should be decreased with the flight Mach number, because the heating ratio is gradually reduced accordingly so as to obtain better engine performance[5]. Thereby for a multi-mode RBCC engine, a variable geometry combustor can balance the combustor area requirements in different modes and at different flight states, and ensure its optimal performance at all modes. However, the harsh operating environment of the combustor increases the difficulties in implementation of variable geometry combustor. An evaluation on performance improvement is necessary before application of a variable geometry combustor in RBCC, considering the cost for development of reliable dynamic sealing in a combustor under a high temperature and high pressure and the increase in weight and size of the actuators and control units.

In our previous work, RBCC performances in the ramjet mode of the Ma 2-6 under variable combustor configurations were studied through numerical simulations and experimental tests[6]. It is showed that the fuels can burn more sufficiently and thus the engine performance can be improved in a RBCC having geometric throats varying in the Ma 2-6. The results arouse interest in implementing a variable geometry combustor in RBCC, and furthermore optimizing RBCC engine performance in a whole flight range. Li's studies [7] on the fixed geometry RBCC combustor in the ramjet mode show that increase of fuel injection positions can improve the performances at off-design conditions, but may result in certain engine performance loss at the design state. Especially at low flight Mach numbers (under eject mode and eject-ramjet mode), RBCC engine with an accelerating climbing trajectory would have worse performance due to a very high fuel consumption [8], which limits the competitiveness of RBCC for self-acceleration missions. In order to cope with the performance losses at low flight Mach number, one has paid attention again to matching between combustor configuration and secondary burning organization. In principle, the configuration of combustor of a wide range operating RBCC should accommodate the combustion organization and performance improvement demands according to inflow conditions. At the low Mach number stage of ramjet mode, the equivalent ratio of the secondary fuel can be increased by changing the expansion ratio of combustor, and the specific impulse of the engine can be increased, premising thrust demand by decreasing the mass flow rate of rocket. Therefore, the variable geometry combustor can be used to reduce the primary rocket mass flow rate at the low Mach number stage of ramjet mode and complete the transition of the rocket-ramjet mode to pure ramjet mode at a low Mach number as early as possible, so as to improve the low Mach number performance of the engine and better expand the application range of RBCC engine.

Moreover, coupling between the inlet/exhaust and the combustor also exerts impacts on a wide operating RBCC engine[9]. Aimed to study the performance of RBCC engine with a variable geometry combustor under the operating constrains of inlet/exhaust at low Mach number, this paper has completed three dimensional CFD simulation in a full flow path of RBCC including the fore-airframe and aft-airframe of a flight vehicle. Validation has been undertaken in the paper. Firstly, the performance of variable geometry RBCC engine in rocket-ramjet mode has been studied under the inflow conditions of Ma2 and Ma3. Then aiming at the Ma3 inflow condition, the performance of variable geometry RBCC engine under different injection strategies has been simulated in detail, and the possibility of the transition of the combustor from rocket-ramjet mode to pure ramjet mode under different combustion organization strategies has also been studied.

2. Variable geometry RBCC engine configurations

The structured dimensions of the variable geometry RBCC under Ma2 and Ma3 inflow conditions are listed in table 1, obtained by a thermodynamic analysis[10]. With the increase of flight Mach number, the inlet contraction ratio, combustor expansion ratio and geometric throat expansion ratio decrease

gradually, while the corresponding nozzle expansion ratio increases gradually. The variable geometry engine is equipped with a two-dimensional three-wave system inlet. The inlet satisfies the inflow of range of Ma2-7 through the transition of cowl lip and inlet throat, and the inlet configurations for flight Ma2 and Ma3 are shown in Fig. 1.

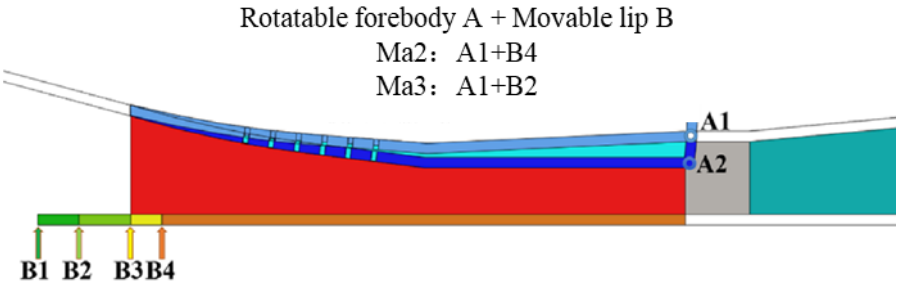

Fig 1. Inlet configurations

Table 1. Parameters of the RBCC configurations

Ma_0	Inlet contraction ratio	Combustor expansion ratio	Throat expansion ratio	Nozzle expansion ratio
2	3.8	3.5	2.9	1.5
3	3.8	2.8	2.3	1.8

The combustor adopts a single-side expansion variable geometry with a geometric throat, which adapts to varied heating ratio according to the wide inflow condition by simultaneously manipulating the combustor to demanded expansion ratio and geometric throat. The combustor configurations for flight Ma2 and Ma3 are shown in Fig. 2. Secondary fuel is injected into the ram combustor along flow path in a flexible combination of three positions, in which the isolator strut and fuel pylon 1 are fixed and fuel pylon 2 is movable along with the top plate of the combustor.

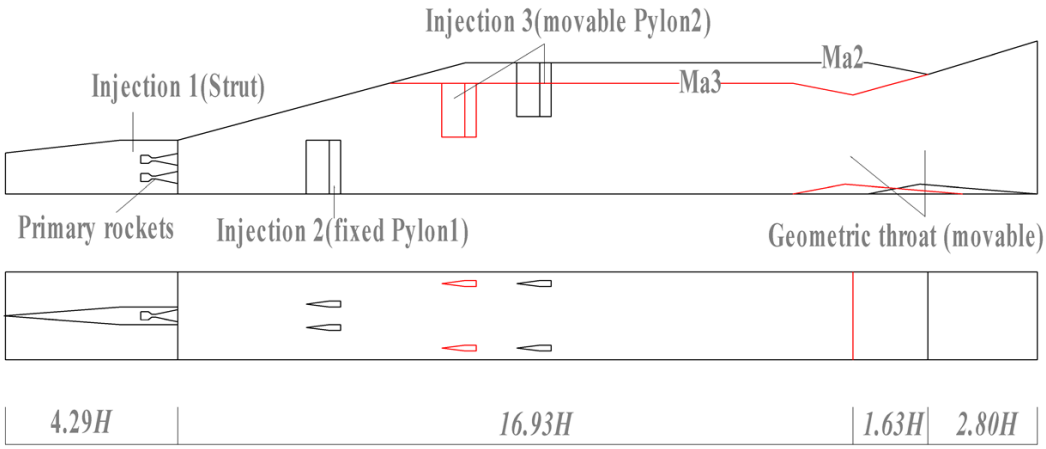

Fig 2. Variable geometry combustor configurations

Also the nozzle is structured having a variable expansion ratio. The expansion ratio is adjustable in a range of 1.5-2.2. Fig. 3 shows nozzle configurations for flight Ma2 and Ma3. A full expansion in the nozzle reaches through varying the area ratio to a desired value at a given flight Mach number.

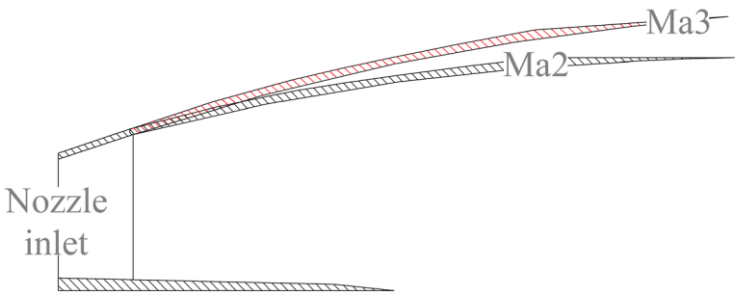

Fig 3. Variable geometry nozzle configurations

3. Numerical methods

References [9, 11, 12] show that Reynolds-averaged Navier-Stokes (RANS)-based CFD modeling is widely used for dual-mode scramjets and RBCC engines. In this paper, the nonlinear RANS equations were solved by using the cubic k-ε turbulence model in CFD++, an unstructured three-dimensional fluid calculation software [13]. In [12, 14, 15], this model was used to simulate the combustor of the HIRIRE-2 scramjet engine, and the model results were consistent with the experimental data.

The Eulerian Dispersed Phase (EDP) model is utilized to simulate the spray of liquid kerosene as the secondary fuel in a gaseous medium. In this paper, turbulence-chemistry interactions were neglected which may result in certain deficiencies in the prediction of ignition delay times. Considering steady state simulations aimed in this study, turbulence-chemistry interactions should not play a crucial role. In the present work, $C_{10}H_{22}$ [16] was selected as kerosene, and a multi-step quasi-global chemical kinetics model proposed by Westbrook [17] was used for the chemical kinetic calculations. This model consists of 10 species and 12 finite rate reactions, as listed in Table 2.

Table 2. Quasi-global chemical kinetics model for kerosene fuel [17]

Reaction	*A*	*b*	*E*	η_F	η_O
$C_{10}H_{22}+5O_2=>10CO+10H_2$	4.50E+09	0	1.256E+08	0.25	1.5
$H+O_2=O+OH$	2.20E+11	0	7.032E+07	1.0	1.0
$H_2+O=H+OH$	1.80E+07	1	3.725E+07	1.0	1.0
$O+H_2O=OH+OH$	6.80E+10	0	7.702E+07	1.0	1.0
$OH+H_2=H+H_2O$	2.20E+10	0	2.135E+07	1.0	1.0
$CO+OH=CO_2+H$	1.50E+04	1.3	3.349E+06	1.0	1.0
$CO+O2=CO_2+O$	3.10E+08	0	1.574E+08	1.0	1.0
$CO+O+M=CO_2+M$	5.90E+09	0	1.716E+07	1.0	1.0
$OH+M=O+H+M$	8.00E+16	-1	4.341E+08	1.0	1.0
$O_2+M=O+O+M$	5.10E+12	0	4.814E+08	1.0	1.0
$H_2+M=H+H+M$	2.20E+11	0	4.018E+08	1.0	1.0
$H_2O+M=H+OH+M$	2.20E+13	0	4.395E+08	1.0	1.0

Experimental pressures at the combustor wall under Ma 3 inflow condition have been used to verify the CFD model and simulation method in a variable geometry combustor[6]. Fig. 4 shows that pressures on the sidewall of the combustor from three dimensional numerical simulation fit the experiment data quite well, moreover CFD simulation has also captured a slight oscillation of the pressure at the fuel pylons and a slight decrease of the pressure caused by heat release in the measured pressures.

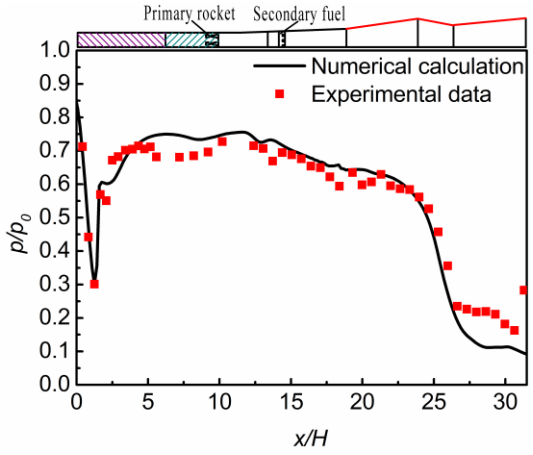

Fig 4. Numerical simulation validation through measured pressure

4. Results and discussion

Table 3 lists operation parameters for the cases to be simulated including flight Mach number, mass flow rate and Oxygen/fuel ratio of the primary rocket, and secondary fuel distributions. For all five cases, the total equivalence ratio remained a value of 1 as shown in Table 3, while the secondary fuel was fed in each case having varied both injected positions and local equivalence ratios. In consideration of the lower total temperature and thus a lower combustion efficiency in the case of Ma2 inflow, a greater rocket mass flow rate (0.2 kg/s) was adopted for Ma2 inflow to ensure its high efficiency combustion, compared to Ma3 inflow. Meanwhile, the secondary fuel was all injected downstream through fuel pylons, considering the low back-pressure resistance capability of inlet at Ma2 inflow. On contrast, the distance along flow path required to evaporate and mixing for the secondary fuel are decreased, and hereby brings a less ignition delay time demands because of the increase of the total temperature of the inflow at Ma3. Therefore, the case Ma3_1 and case Ma3_2 were arranged with the rocket at a lower flow rate and shut off respectively, in order to study the specific impulse performance improvement by throttling the primary rocket and even by shutting off the rocket. The both cases remained the same secondary fuel distribution as the case Ma2. Also the case Ma3_3 was arranged with the same rocket mass flow rate as the case Ma3_1 to reveal the effects of secondary fuel injection on secondary combustion and engine performance by using a varied local equivalence ratio. Similarly, the case Ma3_4 applied the same secondary fuel distribution as the case Ma3_3 but with the rocket shut off.

Table 3. Operation condition parameters

Case	Ma_0	$\dot{m}_{rocket}$	O/F ratio	ER	Injection scheme Strut+Pylon1+Pylon2
Ma2	2	0.20	2.6	1	0+0.6+0.4
Ma3_1	3	0.12	2.6	1	0+0.6+0.4
Ma3_2	3	0	-	1	0+0.6+0.4
Ma3_3	3	0.12	2.6	1	0.2+0.4+0.4
Ma3_4	3	0	-	1	0.2+0.4+0.4

4.1. Full flow path matching in rocket-ramjet mode

Fig. 5 shows the pressure along inner flow path in the rocket-ramjet mode. A stable pressure profile is established in the combustor for both cases in the rocket-ramjet mode. The secondary fuel into the combustor is ignited and burned aided by a high-temperature rocket jet. Since the fuel in the combustor burns under the high-temperature rocket jet, the combustor pressure is stable at a high level. Meanwhile, a pre-combustion shock train will be formed in the isolator section to decelerate the supersonic flow compressed by the inlet in order to match the higher pressure of the combustor. In the combustor, the pressure drops due to the acceleration of subsonic airflow under the effect of heat release. Because of the presence of geometric throats in the variable geometry combustor, the high

temperature gas after combustion passes through the geometric throat and is accelerated to the supersonic state into the nozzle, accompanied by further pressure reducing. In Fig. 5, the pressure rise ratio in the combustor of case Ma2 is about 2.3, which is lower than the highest pressure rise ratio 3.7 in the case Ma3_1. It shows that with the increase of the flight Mach number, the total pressure of inflow will rise sharply, and the followed combustion heat release of the fuel in the combustor will decelerate the airflow to a higher pressure, which is beneficial to the combustion heat release of fuel.

Fig. 6 shows the Mach number along inner flow path in the rocket-ramjet mode. It is seen that the gas in the combustor is completely in subsonic and its Mach number is low under the dual effects of combustion heat release and geometric throat. The Ma distribution also shows that the pre-combustion shock train of the case Ma2 starts basically at the bleed position of the inlet, while the air has completely been reduced to subsonic state before the isolator section and further decelerated in the isolator section due to the friction effect. For case Ma3_1, the air is still in supersonic at the entrance of the isolator section, and decelerates to subsonic due to the pre-combustion shock train in the isolator section. At the entrance of the combustor, the air decelerates significantly to subsonic because of the sudden expansion of the combustor caused by the rocket strut; after the fuel injection position, the flow in the combustor accelerates slowly as the combustion heat release proceeds; finally, it is choked at the geometric throat position and further accelerated into supersonic in the nozzle. That case Ma3_1 has a lower chamber velocity than the case Ma2, and corresponds to a higher chamber pressure rise ratio indicates a more sufficient combustion heat release in case Ma3_1.

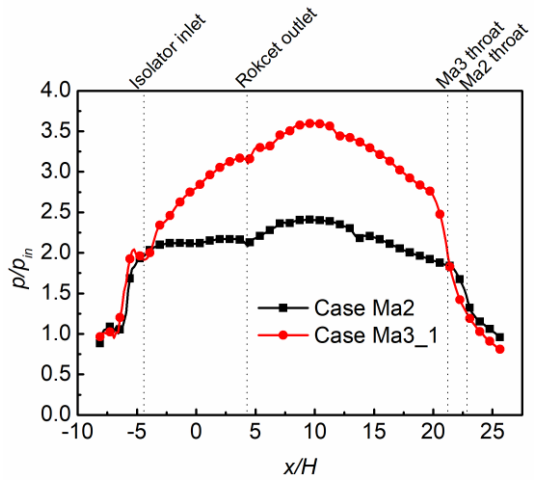

Fig 5. Pressure along inner flow path in rocket-ramjet mode

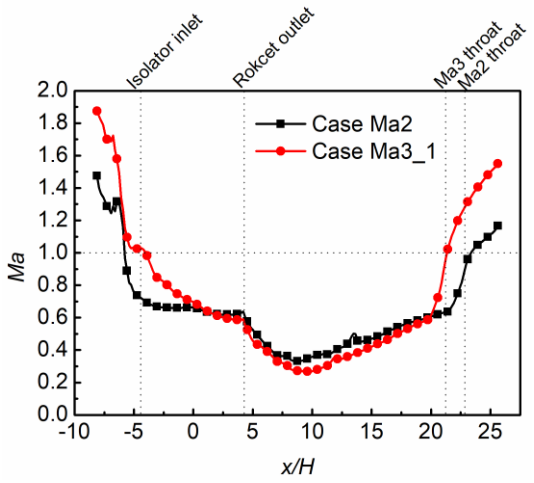

Fig 6. Mach number along inner flow path in rocket-ramjet mode

Fig. 7 shows the Ma⩾1 field of the engine operating in the rocket-ramjet mode. In the case Ma2, the air in the isolator section is completely in a subsonic state. In order to match the pressure in the combustor, a normal shock is formed near the inlet exit due to the low total pressure of the inflow. With the increase of the flight Mach number, both the total pressure of the inflow and the back-pressure resistance capability of the inlet are increased. Hereby, there is a complete pre-combustion shock train structure in the isolator section of the case Ma3_1, and the gas in the combustor is completely in a subsonic state. In the case Ma2, the rocket chamber pressure is higher due to a greater rocket mass flow rate, and while the back-pressure of the ramjet combustor is lower. Therefore, the rocket jet is in an under-expanded state and will expand further in the ramjet combustor, which is beneficial to the heat release of the secondary fuel. On contrast, the rocket jet in the case Ma3_1 is in an over-expanded state. At the geometric throat position of the combustor, the geometric choke is formed, and the gas accelerates by through expansion after geometric throat. Under both operating conditions, the back-pressure in the combustor does not affect the start ability of the inlet, which indicates that the combustor is in normal operating condition.

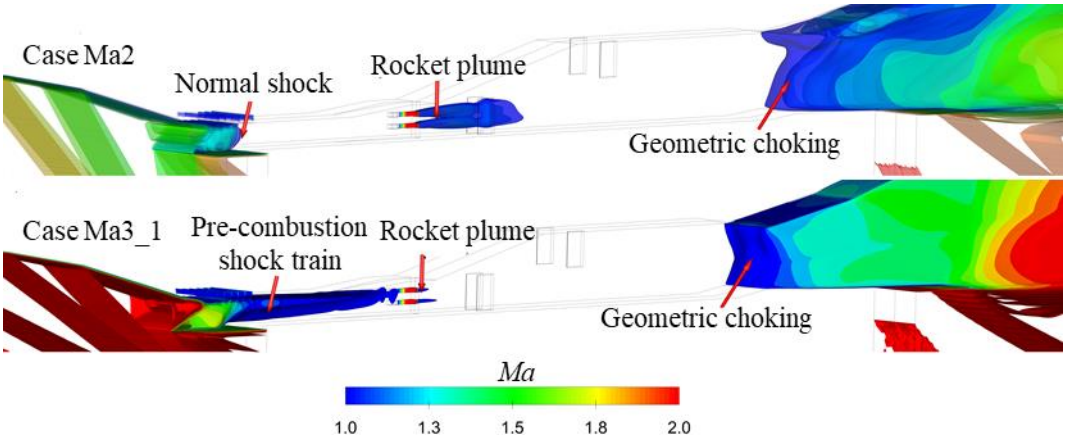

Fig 7. Ma≥1 field of the engine operating in rocket-ramjet mode

The combustion efficiency is given as $\eta_b = \dfrac{T_t(x) - T_{ti}}{T_{AFT} - T_{ti}}$.

Fig. 8 shows the heat release distribution in the rocket-ramjet mode. It is seen that the combustion heat release occurs basically between the combustor entrance and the geometric throat. At the entrance of the combustor, the slightly fuel-rich rocket jet is mixed and burned with the airflow, and a bit heat release is resulted. At the secondary fuel injection position Pylon1, the heat release increases slightly due to the rapid atomization and evaporation combustion of the fuel inside the fuel pylons aided by the rocket jet. In case Ma2, the greater rocket flow rate is favor for the secondary heat release, compared to case Ma3_1. With the combustion and heat release of the fuel outside the fuel pylons, the heat release in the combustor in case Ma3_1 rises sharply so as to form the heat release peak, while the heat release in case Ma2 decreases gradually. Besides with the addition of secondary fuel injected at Pylon 2, the combustion heat release gradually forms another heat release peak in case Ma3_1, and on contrast the heat release is seen also smooth in case Ma2. After the geometric throat, there is further heat release in the nozzle due to the incomplete heat release of fuel in the combustor for both cases with a low inflow total temperature.

Figure 9 shows the combustion efficiency along inner flow path in the rocket-ramjet mode. The combustion efficiency still rises slightly after the geometric throat position, which indicates that heat release still exists in the nozzle. In the rocket-ramjet mode, the combustion efficiencies reach 0.946 and 0.753 respectively for case Ma3_1 and case Ma2.

Table 4 lists the engine performances in the rocket-ramjet mode, including the contributions of ram combustor and rocket to the engine performance. The ram specific impulse is defined as $I_{sp-ram} = \dfrac{F_{ram}}{g_0 \dot{m}_{fuel}}$, and the engine specific impulse as $I_{sp} = \dfrac{F}{g_0(\dot{m}_{fuel} + \dot{m}_{rocket})}$, where the thrust of engine F is a sum of ram thrust plus rocket thrust: $F = F_{ram} + F_{rocket}$.

Previous analysis shows that the inlet back-pressure resistance capability in case Ma2 is limited, thus the engine performance cannot be improved by increasing the combustor pressure. However, it is shown that with the geometric throat in the case Ma2, the inlet and the combustor heat release has been matched. The initial position of the pre-combustion shock train in the case Ma3_1 is close to the inlet exit, and the combustor has high combustion efficiency, which indicates that the performance of ram combustor reaches the engine limit and the inlet can be well matched with the geometric throat of combustor.

In a RBCC engine designed by Wang with a thermal throat combustor, the engine specific impulses were 342s and 882s respectively[18]. The specific impulse performance of the variable geometry engine in this paper is improved by 55% at the Ma2 inflow and 13.5% at the Ma3 inflow. Both engines have the same rocket mass flow rates at the same Mach number.

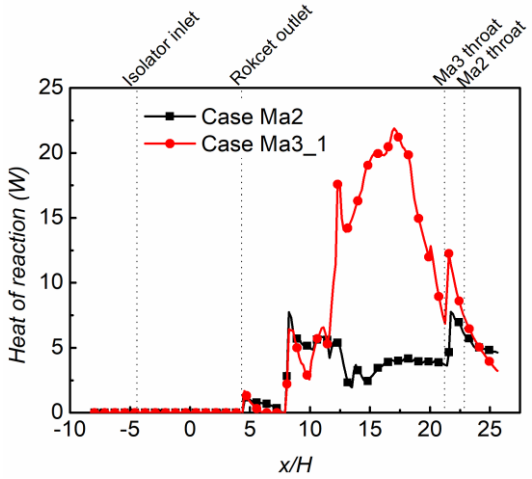

Fig 8. Heat of reaction along inner flow path in rocket-ramjet mode

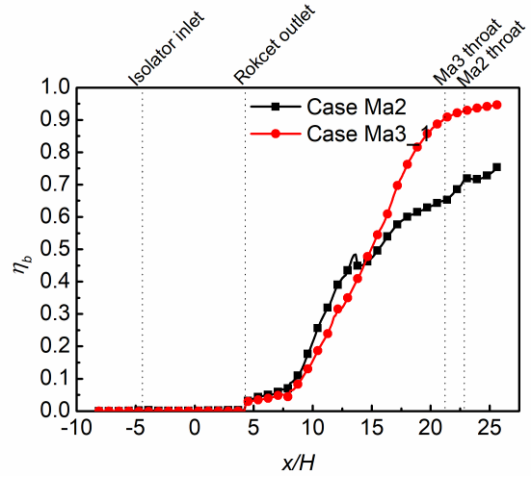

Fig 9. Combustion efficiency along inner flow path in rocket-ramjet mode

Table 4. The performances of engine in the rocket-ramjet mode

Case	F_{ram}	F_{rocket}	F	$I_{sp\text{-}ram}$	I_{sp}
Ma2	1529	532	2061	793	530
Ma3_1	3960	322	4282	1277	1001

4.2. Feasibility of ramjet combustion mode

This section focuses on the feasibility of the engine operating in a pure ramjet mode without rocket jet, so that a low fuel consumption is possible. It is practicable to study matching between inflow and combustion organization at Ma3 because of its higher inflow total temperature and total pressure appropriate for combustion organization without rocket jet.

Fig. 10 shows the pressure along inner flow path in different operating modes under Ma3 inflow condition. The combustor pressure of case Ma3_1, case Ma3_3 and case Ma3_4 are similar, and higher than that of the case Ma3_2. The pressure in case Ma3_1 coincides basically in the isolator and the first half of the combustor with that in the case Ma3_2, while becomes higher in the second half of the combustor. Under the rocket aided ramjet combustion mode, the combustor pressure in case Ma3_1 with more concentrated fuel injection is higher than that in case Ma3_3 with less fuel injected in the isolator section. However, the combustor pressure for case Ma3_2 with the primary rocket shut off is dramatically decreased, and remains throughout lower under the effect of the geometric throat, compared to case Ma3_1. Meanwhile, the pressure in the isolator section remains basically unchanged for case Ma3_2, indicating that no flow separation occurs in the isolator section, and thus the pre-combustion shock train cannot be formed. On contrast, it is inspiring that the flame stabilization effect of the primary rocket is well replaced by injecting 0.2 equivalent ratio fuel into the isolator section for case Ma3_4, which is arranged by shutting off the primary rocket on the basis of the case Ma3_3. Though the pressure in the isolator section and in the front half of the combustor drops slightly, the combustor pressure is maintained at a high level in case Ma3_4.

Fig. 11 shows the Mach number along inner flow path in different operating modes under Ma3 inflow condition. The Mach numbers in case Ma3_1 are basically as the same as in case Ma3_3 in the isolator section, but lower in the combustor due to a concentrated fuel heat release. After the primary rocket is shut off, the secondary fuel in case Ma3_2 cannot be efficiently burned, then the pre-combustion shock train in the isolator section disappears and the viscous drag plays a major role to decelerate the incoming airflow. Meanwhile, the geometric throat of the combustor still maintains the gas in the combustor in subsonic and chokes the gas at the geometric throat position. The secondary fuel in case Ma3_4 maintains a high efficiency combustion, but a slight drop in the chamber pressure results in a shock train in the isolator section to move toward the combustor. Hence the velocity in the front of the

combustor in case Ma3_4 is higher than that in case Ma3_3, while lower in the rear of the combustor due to a weaker acceleration effect by the secondary fuel heat release.

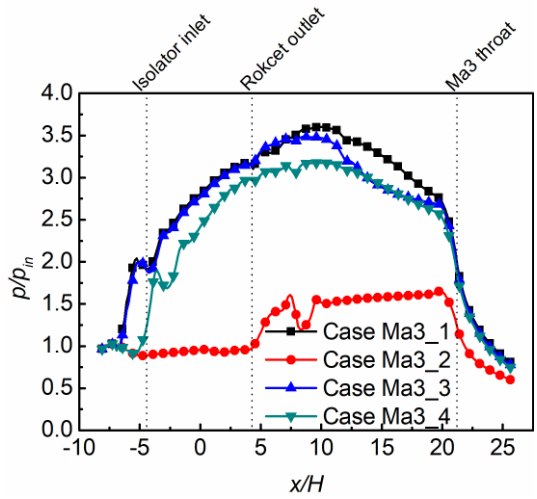

Fig 10. Pressure along inner flow path in different operating modes under Ma3 inflow condition

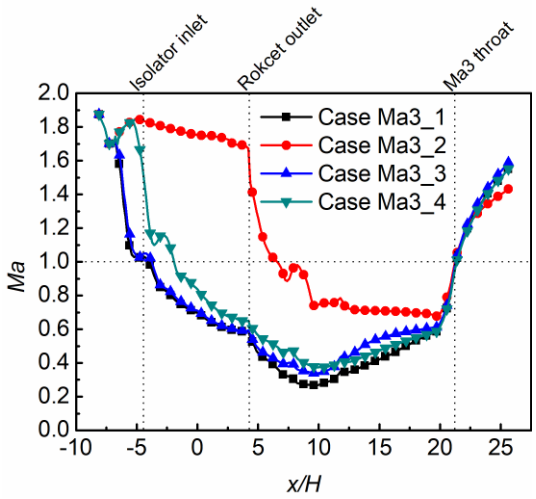

Fig 11. Mach number along inner flow path in different operating modes under Ma3 inflow condition

Fig. 12 shows the Ma≥1 field of the engine in different operating modes under Ma3 inflow condition. The pre-combustion shock trains in case Ma3_1 and case Ma3_3 are basically in the same form, and geometric choking occurs at the geometric throat position. When the rocket is shut off, the secondary fuel burning in case Ma3_2 fails to reach a high-efficiency and no flow separation takes place in the isolator section. Furthermore, its pre-combustion shock train exists in the combustor, and the choking locates near the geometric throat. Comparatively, secondary fuel in case Ma3_4 continues to release heat efficiently but the intensity decreases slightly, which results in the pre-combustion shock train in the isolator section moving backward despite of a geometric choking at the geometric throat position.

Fig. 13 shows the heat release distribution along inner flow path in different operating modes under Ma3 inflow condition. The heat release curves in different operating modes differ greatly, but the heat release is generally concentrated between the rocket exit and the geometric throat of the combustor. The combustion heat release peak in case Ma3_3 is relatively in advance due to a small amount of injection fuel in the isolator section, and its heat release is basically completed after the geometric throat of the combustor, while in case Ma3_1 the fuel heat release still proceeds after the geometric throat. After the primary rocket shuts off, the heat release intensity in case Ma3_2 decreases significantly, and a weak combustion is maintained in the combustor under the effect of the geometric throat. On contrast, the heat release intensity in case Ma3_4 can be maintained in the combustor because its fuel injected into the isolator section functions as a flame stabilization in the low velocity region behind the rocket strut, replacing the effect of the rocket jet. When no efficient flame stabilization by the primary rocket, the fuel heat release decreases greatly in intensity and extends long downstream lasting after the geometric throat.

Fig. 14 shows the combustion efficiency along inner flow path in different operating modes under Ma3 inflow condition. Case Ma3_1 with concentrated secondary fuel injection is characteristic of the highest combustion efficiency. The combustion efficiency is also as high as 0.910 in case Ma3_3. After the primary rocket shuts off, case Ma3_2 could not maintain an efficient combustion, and its combustion efficiency drops sharply to 0.233. Although the combustion intensity is maintained in case Ma3_4, its combustion efficiency still drops to 0.75.

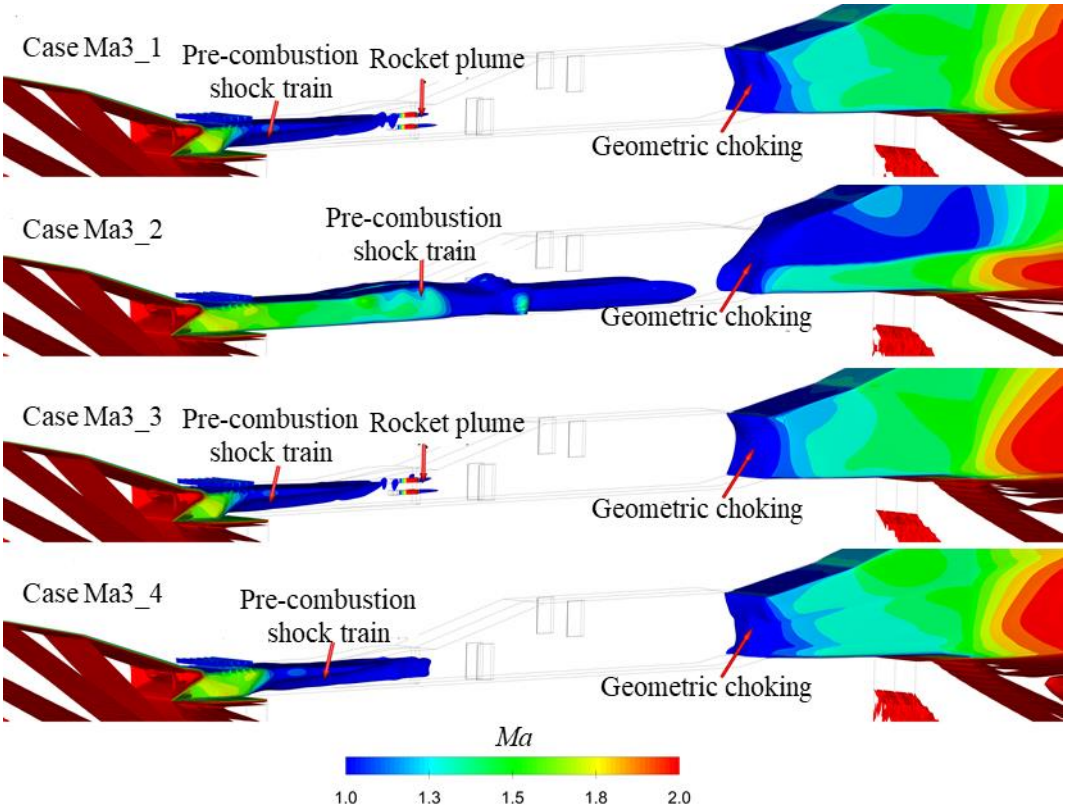

Fig 12. Ma≥1 field of the engine in different operating modes under Ma3 inflow condition

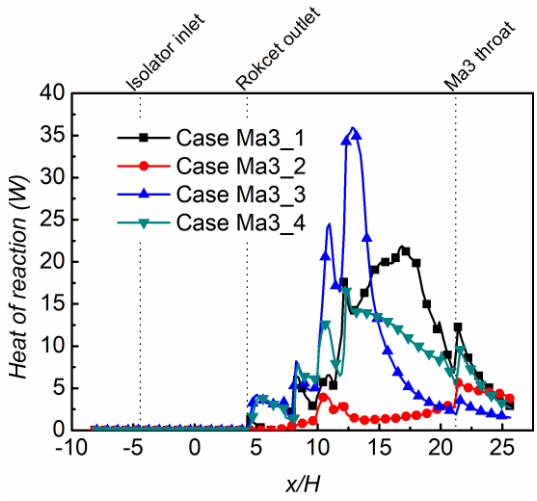

Fig 13. Heat of reaction along inner flow path in different operating modes under Ma3 inflow condition

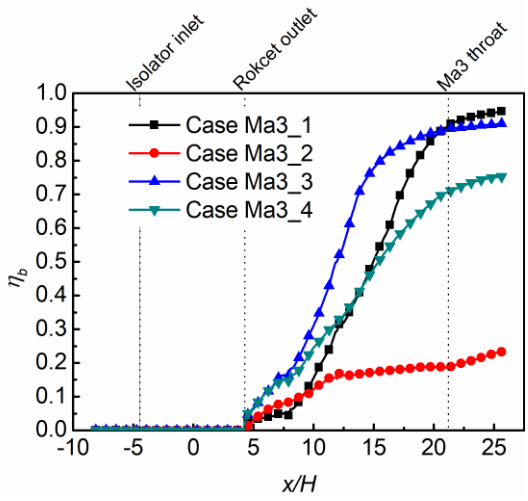

Fig 14. Combustion efficiency along inner flow path in different operating modes under Ma3 inflow condition

Table 5 shows the engine performances in different operating modes under Ma3 inflow condition. Case Ma3_1 with concentrated injected secondary fuel achieves better engine performances than case Ma3_3. In comparison of case Ma3_3 and case Ma3_4, the operation of the primary rocket brings both higher combustion efficiency and higher ram specific impulse of the engine under the same injection strategy, which further illustrates the positive role of the primary rocket in enhancing the efficient combustion heat release of secondary fuel. Though case Ma3_2 fails to organize an efficient combustion and the engine fails to operate properly, the engine still produces thrust under the effect of geometric throat. By the adjustment of the fuel injection strategy, a pure ramjet mode at Ma3 instead of a rocket-ramjet mode has been realized. Though the combustion efficiency decreases in the pure ramjet mode and results in the ramjet specific impulse decreased by 10.2%, compared with the rocket-ramjet mode, the specific impulse of the engine is however inspiringly increased by 14.5%.

Table 5. The performances of engine in different operating modes under Ma3 inflow condition

Case	F_{ram}	F_{rocket}	F	$I_{sp\text{-}ram}$	I_{sp}
Ma3_1	3960	322	4282	1277	1001
Ma3_2	819	0	819	264	264
Ma3_3	3876	322	4198	1250	982
Ma3_4	3554	0	3554	1146	1146

5. Conclusions

In this paper, a variable geometry RBCC engine has been configured and simulated numerically in the full flow path at low inflow Mach number conditions. Under Ma2 and Ma3 inflow conditions, the characteristics of the engine operating in both rocket-ramjet mode and pure ramjet mode have been studied. Transition of combustion mode from rocket-ramjet mode to ramjet mode has been realized at Ma3. Concluding remarks are summarized below.

(1) In the rocket-ramjet mode, the primary rocket has obvious positive effects on flame stabilization and combustion enhancement of secondary fuel. Because of the low total temperature of the inflow at Ma2, the stable combustion of the secondary fuel relies on the assistance of the primary rocket, while a lower mass flow rate of the primary rocket improves the secondary fuel combustion efficiency and results in a higher ramjet specific impulse under the Ma3 inflow condition. Matching of the combustor and inlet/exhaust has been realized under the rocket-ramjet mode.

(2) Under the Ma3 inflow condition, improvement of the combustor performances prefers a concentrated fuel injection rather than a dispersed injection through isolator section and pylons. Furthermore, fuel injected in advance into the isolator section realizes the transition of engine operation from the rocket-ramjet mode to the pure ramjet mode. It is inspiring that the specific impulse of the engine in a pure ramjet mode is increased by 14.5% compared to a rocket-ramjet mode, though the ram specific impulse decreased by 10.2% due to a decreased combustion efficiency in the pure ramjet mode.

References

1. Clark, C., K. Kloesel, and N. Ratnayake. A Technology Pathway for Airbreathing, Combined-Cycle, Horizontal Space Launch Through SR-71 Based Trajectory Modeling. in 17th AIAA International Space Planes and Hypersonic Systems and Technologies Conference. San Francisco, California, AIAA (2011).
2. Daines, R. and C. Segal, Combined Rocket and Airbreathing Propulsion Systems for Space-Launch Applications. Journal of Propulsion and Power. 14(5), 605-612 (1998).
3. Flaherty, K.W., K.M. Andrews, and G.W. Liston, Operability Benefits of Airbreathing Hypersonic Propulsion for Flexible Access to Space. Journal of Spacecraft and Rockets, 47(2), 280-287 (2010).
4. Kodera, M., et al. Multi-Objective Design and Trajectory Optimization of Space Transport Systems with RBCC Propulsion via Evolutionary Algorithms and Pseudospectral Methods. in 52nd Aerospace Sciences Meeting. National Harbor, Maryland, AIAA (2014).
5. Gounko, Y.P. and V.V. Shumskiy, Characteristics of dual-combustion ramjet. Thermophysics and Aeromechanics. 21(4), 499-508 (2014).
6. Ye, J., et al., Investigation of RBCC performance improvements based on a variable geometry ramjet combustor. Acta Astronautica. 151, 874-885 (2018).
7. Li, Y., Thermal Adjustment Mechanism Research on Ejector and Ramjet Mode of RBCC. Northwestern Polytechnical University, Xi'an (2008).

8. Lin, B.-b., et al., Effect of Primary Rocket Jet on Thermodynamic Cycle of RBCC in Ejector Mode. International Journal of Turbo & Jet-Engines. (2017). https://doi.org/10.1515/tjj-2017-0013
9. Shi, L., et al., Numerical analysis of flow features and operation characteristics of a rocket-based combined-cycle inlet in ejector mode. Acta Astronautica. 127, 182-196 (2016).
10. Ye, J., H. Pan, and F. Qin, Investigation on the Applicable Scope of Geometrical Throat in RBCC Variable Structure Combustion Chamber. Journal of Northwestern Polytechnical University. 35(6), 975-982 (2017).
11. Feng, S., et al., Numerical studies for performance improvement of a variable geometry dual mode combustor by optimizing deflection angle. Aerospace Science and Technology. 68, 320-330 (2017).
12. Yentsch, R.J. and D.V. Gaitonde, Numerical Investigation of Dual-Mode Operation in a Rectangular Scramjet Flowpath. Journal of Propulsion and Power. 30(2), 474-489 (2014).
13. METACOMP, CFD++ & CAA User Manual, M. Technologies, Editor. Agoura Hills, CA (2011).
14. Liu, J. and M. Gruber. Preliminary Preflight CFD Study on the HIFiRE Flight 2 Experiment. in 17th AIAA International Space Planes and Hypersonic Systems and Technologies Conference. AIAA (2011).
15. Storch, A., et al. Combustor Operability and Performance Verification for HIFiRE Flight 2. in 17th AIAA International Space Planes and Hypersonic Systems and Technologies Conference. Francisco, California, AIAA (2011).
16. Franzelli, B., et al., A two-step chemical scheme for kerosene–air premixed flames. Combustion and Flame. 157(7), 1364-1373 (2010).
17. Westbrook, C.K. and F.L. Dryer, Simplified Reaction Mechanisms for the Oxidation of Hydrocarbon Fuels in Flames. Combustion Science and Technology. 27(1-2), 31-43 (1981).
18. Yajun, W., Investigation of Ramjet Mode in RBCC for Wide Adaptability based on Thermal Adjustment. Northwestern Polytechnical University, Xi'an (2017).